

# Analysis of a Sleep-Dependent Neuronal Feedback Loop: The Slow-Wave Microcontinuity of the EEG

Bastiaan (Bob) Kemp\*, *Member, IEEE*, Aeilko (Koos) H. Zwinderman, Bert Tuk, Hilbert A. C. Kamphuisen, and Josefien J. L. (Janine) Oberyé

**Abstract**—Increasing depth of sleep corresponds to an increasing gain in the neuronal feedback loops that generate the low-frequency (slow-wave) electroencephalogram (EEG). We derived the maximum-likelihood estimator of the feedback gain and applied it to quantify sleep depth. The estimator computes the fraction (0%–100%) of the current slow wave which continues in the near-future (0.02 s later) EEG. Therefore, this percentage was dubbed *slow-wave microcontinuity* (SW%). It is not affected by anatomical parameters such as skull thickness, which can considerably bias the commonly used *slow-wave power* (SWP).

In our study, both of the estimators SW% and SWP were monitored throughout two nights in 22 subjects. Each subject took temazepam (a benzodiazepine) on one of the two nights. Both estimators detected the effects of age, temazepam, and time of night on sleep. Females were found to have twice the SWP of males, but no gender effect on SW% was found. This confirms earlier reports that gender affects SWP but not sleep depth. Subjectively assessed differences in sleep quality between the nights were correlated to differences in SW%, not in SWP.

These results demonstrate that slow-wave microcontinuity, being based on a physiological model of sleep, reflects sleep depth more closely than SWP does.

**Index Terms**—Aliasing, EEG, estimator, sleep, temazepam.

## I. INTRODUCTION

SLEEP consists of periods of rapid eye movement (REM) and non-REM (NREM) sleep. The depth of NREM sleep varies between and within NREM periods. These variations of NREM-sleep depth are accompanied by synchronous variations of the amplitude of the low-frequency component of the EEG, usually called the slow wave.

Because of this, quantitative studies of NREM sleep are commonly based on slow-wave power (SWP) [1]–[5]. However, the SWP as measured through scalp EEG electrodes can also be influenced by processes that are not related to sleep, such as

anatomical characteristics of the head. Therefore, effects in the power plots do not necessarily reflect effects on sleep. For instance, females have twice the SWP of males, but this does not imply that they really sleep more deeply [5], [6]. This uncertainty also exists when within-subject effects on total duration of NREM-sleep are studied. The amplitude (or power) thresholds that are involved in the computation of durations depend also on nonsleep-related processes: the power thresholds correspond to different sleep depths in different subjects.

These nonsleep-related effects can be partly avoided by applying relative power measures, such as the percentage of the total power that is in the slow-wave frequency band, or the ratio of powers in the slow-wave and alpha band. However, it is not clear how such a ratio would be related to real, physiological, sleep depth. Also, relative power measures are based on frequency analysis, which implies a rather limited time resolution when compared to the frequent and abrupt sleep depth variations that can occur in, for instance, sleep apnea patients.

Some physiological models of NREM sleep [7]–[9], [4] suggest a different method that would not suffer from these drawbacks. These models describe how NREM sleep depth is related to the neuronal mechanism that generates slow waves. This mechanism is essentially feedback through closed loops in neuronal networks and/or through the interplay between ion currents in single cells. It is suggested that NREM sleep depth modulates the gain of the feedback loops [9]. According to this model, the *sleep-related* variations in SWP result from variations in the feedback gain. Therefore, a direct estimate of slow-wave feedback gain would be most closely related to real physiological sleep depth. In particular, this estimate would not be biased by the nonsleep-related anatomical parameters that do bias SWP. Also, because the models are in the time domain, the estimator would not be limited by the time resolution of frequency analysis.

In this article we describe for the first time the model-based estimator of the slow-wave-feedback gain in full detail. The following sections enable full understanding and implementation of both the model and the feedback gain estimator. These can be applied to any EEG rhythm [10]–[16]. However, the actual values of sampling intervals, filter frequencies and artifact detection thresholds as given in the present article are specific to the analysis of slow waves in the EEG.

Preliminary implementations of the algorithm demonstrated its value in the analysis of EEG components other than slow waves [10]–[16]. The algorithm was first applied to slow waves in a study addressing the effects of age and gender in an extremely healthy population [6]. In order to further illustrate the

Manuscript received January 7, 1999; revised April 6, 2000. Asterisk indicates corresponding author.

\*B. Kemp is with the Center for Sleep and Wake Disorders, MCH Westeinde Hospital, P.O. Box 432, NL-2501 CK Den Haag, The Netherlands. He is also with the Department of Neurology and Clinical Neurophysiology of Leiden University Medical Center, P. O. Box 9600, NL-2300 RC Leiden, The Netherlands (e-mail: K@HSR.NL).

A. H. Zwinderman is with the Department of Medical Statistics of Leiden University, NL-2300 RC Leiden, The Netherlands.

B. Tuk and J. J. L. Oberyé were with the Division of Pharmacology, Leiden/Amsterdam Center for Drug Research, Leiden University, NL-2300 RA Leiden The Netherlands.

H. A. C. Kamphuisen, retired, was with the Center for Sleep and Wake Disorders, MCH Westeinde Hospital, P.O. Box 432, NL-2501 CK Den Haag, The Netherlands.

Publisher Item Identifier S 0018-9294(00)08016-2.

practical value of the estimator, we monitored slow-wave feedback gain as well as SWP throughout two nights in 22 subjects having sleep complaints. We analyzed whether slow-wave feedback gain: 1) reflects sleep depth variations that are also visible as variations in SWP caused by the ultradian rhythm (time of night), aging, and the use of sleep medication; 2) reflects the (possibly not-sleep-related) gender effect on SWP. We also compared the results to those that can be obtained by relative SWP analysis.

An important issue in sleep medicine is the correlation of subjective measures (as derived from sleep quality questionnaires) with the total duration of NREM-sleep, as computed by, for instance, thresholding overnight SWP plots. To date, no such correlation has been found within individuals: the objectively measured total duration of NREM-sleep does not yet support the difference between a (subjectively) good and a bad night in one subject. In our view, this may be partly due to the fact that these objective measures do not use the information from the physiological models mentioned above. The analysis of slow-wave feedback gain, being based on a physiological sleep model, might show correlations not revealed by more traditional measures. We have, therefore, also analyzed whether the subjective difference between the two recorded nights was correlated with the difference in NREM-sleep duration as computed by thresholding slow-wave feedback gain plots. Since, in this study, temazepam was taken on one of the nights, this analysis essentially determines whether those found by objective measures to be drug responders are also the responders as determined by subjective measures.

## II. THE FEEDBACK MODEL: GENERATION OF SLOW WAVES IN THE EEG

The derivation of the feedback gain estimator is based on a simple mathematical model of the slow-wave generating feedback system. This model describes three essential characteristics of the above-mentioned physiological models: 1) the existence of a low-frequency feedback loop in which the feedback gain is proportional to sleep depth; 2) unpredictable activity from external sources drives the loop; 3) increased feedback gain corresponds to larger SWP. These characteristics can be implemented in various practical mathematical models. Physiological knowledge does not provide clear criteria to select between these models. Therefore, we have implemented a variety of models, based on the three above mentioned characteristics. The models differed in types of low-frequency filters in the feedback loop, in random processes driving the filter, and in location of the feedback gain. We selected the model that most realistically simulated EEG.

Fig. 1 shows a block diagram of that model. Standard white noise,  $\dot{w}(t)$ , drives a feedback loop containing a resonance filter,  $G(f)$ , and a feedback-gain,  $p(t)$ . This feedback gain represents sleep depth. The feedback loop produces an output signal,  $\dot{u}(t)$ . The resonance filter passes only the rhythmic (in this case, the slow-wave) component,  $s(t)$ , of this output signal. The feedback gain determines which fraction of this component actually continues in the near-future output signal. The output

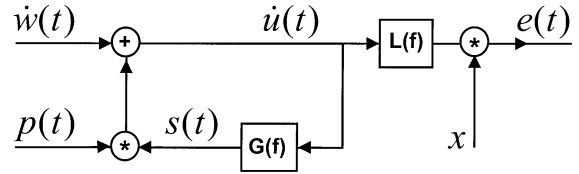


Fig. 1. Model of the neuronal generation of slow-wave EEG. Neuronal-group activity under the electrode is represented by  $\dot{u}(t)$ .  $G(f)$  represents frequency-selective neuronal feedback pathways that can carry the slow-wave component,  $s(t)$ , of this activity to the near-future activity under the same electrode. Sleep-dependent activation of these pathways is represented by the feedback gain,  $p(t)$ . Stronger activation corresponds to larger  $p(t)$ , which makes a larger fraction of the slow-wave component continue in the near-future activity. The external input activity to the system is represented by random white noise,  $\dot{w}(t)$ .  $L(f)$  and  $x$  describe how the activity under the electrode is low-pass filtered and attenuated, respectively, before it is recorded as scalp EEG,  $e(t)$ .

signal passes a low-pass filter,  $L(f)$ , and a not-sleep-related amplification factor,  $x$ , before being recorded as scalp EEG,  $e(t)$ . A similar model was proposed earlier [16] for the alpha rhythm in the EEG. Simulations by the model [10], [14], [16] show a waxing and waning rhythm, similar to the behavior of narrow-band filtered white noise. Increasing sleep depth was simulated by increasing  $p(t)$  while keeping all other parameters constant. Therefore, the model is stationary except for  $p(t)$  which is to be estimated. The simulations were visually nearly indistinguishable from real EEG.

The resonance filter,  $G$ , is linear, with the following transfer function in the frequency ( $f$ ) domain:

$$G(f) = \frac{1}{1 + j \cdot Y(f)} \quad \text{with } Y(f) = \frac{f_0}{B} \cdot \left( \frac{f}{f_0} - \frac{f_0}{f} \right) \quad (1)$$

where  $j$  is the complex operator, and  $f_0 = 1$  Hz and  $B = 1.5$  Hz are the center frequency and bandwidth, respectively. The resulting  $-3$  dB frequencies of the resonance filter are 0.5 Hz and 2 Hz. The roll-off at both ends is only 6 dB/octave, which implies that a considerable part of the signal below 0.5 Hz and above 2 Hz is also passed. These settings roughly correspond to the frequency content of slow waves. They also result in simulated signals and power spectral densities that best resemble those of actual EEG recordings [14]. Note that  $G(f_0) = 1$ , and all other frequencies are attenuated as well as changed in phase. The equivalent notation in the complex-frequency ( $s = j2\pi f$ ) domain reads

$$G(s) = \frac{2\pi Bs}{s^2 + 2\pi Bs + (2\pi f_0)^2} = \frac{2\pi Bs}{(s+a) \cdot (s+b)}$$

with

$$a = \pi \left[ B + \sqrt{B^2 - (2f_0)^2} \right] \quad \text{and} \\ b = \pi \left[ B - \sqrt{B^2 - (2f_0)^2} \right]. \quad (2)$$

In all our applications we have  $B < 2f_0$ , which makes  $a$  and  $b$  complex constants. In the time ( $t$ ) domain, the resonance filter is specified by its impulse response function:

$$g(t) = 2\pi B \cdot \frac{b \cdot e^{-bt} - a \cdot e^{-at}}{b - a}. \quad (3)$$

In the open-loop situation, i.e.,  $p(t) = 0$ , the filter produces the rhythmic component,  $s(t)$ , by convoluting the white-noise input as follows:

$$\begin{aligned} s(t) &= \int_{\tau=-\infty}^t g(t-\tau) \cdot \dot{w}(\tau) \cdot d\tau \\ &= \int_{\tau=-\infty}^t g(t-\tau) \cdot dw(\tau). \end{aligned} \quad (4)$$

The last part of this equation is a Wiener integral involving increments,  $dw(\tau)$ , of the standard Wiener process,  $w(t)$ . The formal derivative of this process is the white Gaussian noise,  $(dw(t)/dt) = \dot{w}(t)$ , which is in the first part of the equation. White Gaussian noise has infinite power and bandwidth, which would complicate the formal derivation and a straightforward discretization of the analyzer. The Wiener process has finite power. Its increments,  $w(t + \Delta) - w(t)$ , are mutually independent and simply have a Gaussian distribution with mean 0 and variance  $\Delta$  [18, chapter 1]. These properties enable simple and straightforward derivation of the analyzer in paragraph III. A Wiener integral is formally defined as the limit of approximating discrete-time sums, in this case as follows [18, chapter 4.3]

$$\begin{aligned} s(t) &= \int_{\tau=-\infty}^t g(t-\tau) \cdot dw(\tau) \\ &= \lim_{\Delta \rightarrow 0} \sum_{k=-\infty}^{N-1} g(N\Delta - k\Delta) \cdot [w(k\Delta + \Delta) - w(k\Delta)]. \end{aligned} \quad (5)$$

This formulation provides clear suggestions on how to implement the continuous-time components of the model in discrete time (Section III). For these two reasons, we have based the model formulation as well as the derivation of the analyzer on Wiener increments,  $dw(\tau)$ . A more detailed and complete discussion on this subject can be found for instance in [18, chapters 1, 4 and 6.5].

The open-loop power of  $s(t)$  can thus be derived as follows:

$$\begin{aligned} P_{s(t)|p(t)=0} &= E[s^2(t)|p(t) = 0] \\ &= E \left[ \int_{\tau=-\infty}^t g(t-\tau) dw(\tau) \right]^2 \\ &= \int_{\tau=-\infty}^t g^2(t-\tau) E[dw(\tau)]^2 \\ &= \int_{\tau=-\infty}^t g^2(t-\tau) d\tau \\ &= \int_{\tau=0}^{\infty} g^2(\tau) d\tau = \pi B \end{aligned} \quad (6)$$

in which  $E$  denotes the expected value operator. Note, that the fourth equality in (6) is true because of the above-mentioned property of the Wiener increments: the variance of  $dw(\tau)$  over an interval  $d\tau$  equals  $d\tau$  [18, chapter 4.3].

In the general, closed-loop situation, the filter produces the rhythmic component,  $s(t)$ , by convoluting  $\dot{u}(t) = (du(t)/dt)$  as follows:

$$\begin{aligned} s(t) &= \int_{\tau=-\infty}^t g(t-\tau) \cdot \dot{u}(\tau) \cdot d\tau \\ &= \int_{\tau=-\infty}^t g(t-\tau) \cdot du(\tau). \end{aligned} \quad (7)$$

According to Fig. 1, this rhythmic component is amplified by a gain factor,  $p(t)$ , before being added to the new noise input,  $\dot{w}(t)$ , thus producing the new output signal,  $\dot{u}(t)$ , of the closed feedback loop. So,  $\dot{u}(t) = p(t) \cdot s(t) + \dot{w}(t)$ . The equivalent formulation based on Wiener increments reads

$$du(t) = p(t) \cdot s(t)dt + dw(t) \quad (8)$$

in which the forward increment  $dw(t) = w(t + dt) - w(t)$  is independent of  $s(t)$  because the latter results from a causal feedback filter accumulating only previous increments: see equation (5). This does not affect the simulated signals because these result from convolutions in which the contribution of the most recent increment,  $dw(t)$ , is infinitely small. Physiologically, the provision makes sense because the neuronal feedback pathways will surely involve a time delay. Observing  $du(t)$  is equivalent to observing the EEG,  $e(t)$ , because the filter  $L(f)$  is known. Therefore, from now on, we designate  $du(t)$  to be the observations and (8) is the observations model.

We will now describe some characteristics of the model in the frequency domain. The closed-loop transfer function from  $\dot{w}(t)$  to  $\dot{u}(t)$  depends on  $p(t)$ . For constant  $p(t) = p$ , it reads as follows in the frequency domain:

$$U(f) = \frac{1}{1 - p \cdot G(f)}. \quad (9)$$

In the model, this transfer function is driven by standard (i.e., having a power spectral density of 1) white noise  $\dot{w}(t)$ . Therefore, the power spectral density of the output,  $\dot{u}(t)$ , equals

$$|U(f)|^2 = \frac{1 + Y^2(f)}{(1 - p)^2 + Y^2(f)}. \quad (10)$$

For  $p = 0$  (no feedback), the power spectral density is flat. For  $p = 1$ , it has an infinite peak at  $f_0$ . For any value of  $p$ ,  $Y(f)$  becomes infinitely large at very low or very high frequencies, so the power spectral density at those frequencies equals 1. With  $f$  going to  $f_0$ ,  $Y(f)$  goes to 0 and the power spectral density monotonously rises to a peak value of  $1/[(1 - p)^2]$ . This shows that our choice of  $G(f)$  produces only peaks in the power spectrum, and no dips. This is consistent with actual EEG power spectral densities, which also consist of a fairly smooth baseline spectrum that can show peaks (for instance, at alpha, spindle or slow-wave frequencies) that are not accompanied by a decrease of the spectrum at other frequencies. This fact is a major argument for our particular choice of the feedback filter  $G(f)$ . Different filters, such as delay lines or higher-order resonance filters, can also produce peaks in the spectrum but these are always accompanied by dips at other frequencies.

The closed-loop transfer function from  $\dot{w}(t)$  to  $s(t)$  reads

$$S(f) = G(f) \cdot U(f) = \frac{G(f)}{1 - p \cdot G(f)} = \frac{1}{1 - p + j \cdot Y(f)}. \quad (11)$$

This transfer function is identical to the open-loop transfer function of (1), except that the bandwidth is  $B \cdot (1 - p)$  instead of  $B$ , and the gain at  $f_0$  is  $1/(1 - p)$  instead of 1. Therefore, the closed-loop power of  $s(t)$  can directly be deduced from (6). It equals

$$P_{s(t)|p(t)=p} = \frac{\pi B}{1 - p}. \quad (12)$$

Finally, the output,  $\dot{u}(t)$ , of the closed loop passes a first-order low-pass filter and an unknown constant amplification factor,  $x$ , resulting in the EEG,  $e(t)$ . The factor  $x$  affects EEG (and slow-wave) power and represents biological attenuators (such as the skull), electronic amplifiers, as well as the possibility that the white noise input is stronger or weaker than standard white noise. The transfer function of the low-pass filter reads [16]

$$L(s) = \frac{2\pi f_c}{s + 2\pi f_c} \quad (13)$$

where  $f_c = 1.8$  Hz is the  $-3$  dB cutoff frequency.

### III. MODEL-BASED ESTIMATION OF THE NEURONAL-FEEDBACK GAIN: SLOW-WAVE MICROCONTINUITY

The model's feedback gain,  $p(t)$ , represents sleep depth. We will, therefore, quantify sleep depth by estimating the feedback gain. The discrete-time maximum-likelihood estimator can be derived as follows. Discrete-time intervals,  $\Delta$ , are 0.02 s in the present application (EEG slow waves), corresponding to a sampling frequency of 50 Hz. This frequency is sufficiently high for an accurate representation of the slow-wave component. Selecting still higher sampling frequencies increases the risk of bias by unknown technical or physiological high-frequency filters that are not accounted for by the model. The continuous-time observations,  $du(t)$  over an interval  $0 \leq t < T$ , are sampled with sample counter,  $k$ , resulting in discrete-time observations,  $Du(k\Delta) = u(k\Delta + \Delta) - u(k\Delta)$  over an interval  $[0 \leq k\Delta < N\Delta - \Delta]$ , with  $N\Delta = T$ . We assume for the moment (see Section IV) that this interval is short when compared to the dynamics of  $p(t)$ , so that  $p(t) = p|_{0 \leq t < T}$ . We further note that the sampling interval,  $\Delta$ , is short when compared to the slow-wave frequencies (being around 1 Hz), so that we assume that  $s(t) = s(k\Delta)$  in the interval,  $[k\Delta - \Delta \leq t < k\Delta]$ . The discrete-time equivalent of the model is then obtained by integrating (8) and reads

$$Du(k\Delta) = p \cdot s(k\Delta) \cdot \Delta + Dw(k\Delta) \quad (14)$$

in which  $Dw(k\Delta) = w(k\Delta + \Delta) - w(k\Delta)$  is the increment of the standard continuous-time Wiener process,  $w(t)$ , over the time increment,  $\Delta$ , and, therefore, has a Gaussian distribution with mean 0 and variance  $\Delta$ . As in the continuous-time model, the increments  $Dw(k\Delta)$  are independent of  $s(k\Delta)$  because

$s(k\Delta)$  is produced by a causal feedback loop while  $Dw(k\Delta)$  is defined as a forward increment with respect to  $t = k\Delta$ . We finally assume that the initial state,  $\Gamma(0)$ , of the feedback filter,  $G(f)$ , is known so that its output,  $s(k\Delta)$ , can be updated on-line from the input,  $Du(k\Delta - \Delta)$ . The likelihood of  $[Du(k\Delta): 0 \leq k < N - 1]$ , which is of the observations over the full interval, given the value of  $p$ , can be factorized according to Bayes' rule [18, Ch. 4.5] into a product of, in this case Gaussian, distributions

$$\begin{aligned} f [Du(k\Delta): 0 \leq k < N - 1 | \Gamma(0), p] &= \prod_{k=0}^{N-1} [Du(k\Delta) | [Du(m\Delta): 0 \leq m < k], \Gamma(0), p] \\ &= \prod_{k=0}^{N-1} [Du(k\Delta) | s(k\Delta), p] \\ &= \prod_{k=0}^{N-1} \left[ \frac{1}{\sqrt{2\pi\Delta}} \cdot \exp \left[ -\frac{[Du(k\Delta) - p \cdot s(k\Delta) \cdot \Delta]^2}{2\Delta} \right] \right] \\ &= \frac{1}{\sqrt{2\pi\Delta}} \cdot \exp \sum_{k=0}^{N-1} \left[ -\frac{[Du(k\Delta) - p \cdot s(k\Delta) \cdot \Delta]^2}{2\Delta} \right]. \end{aligned} \quad (15)$$

For the third equality, we have used (14) and the Gaussian distribution of  $Dw(k\Delta)$ . The value of  $p$  that maximizes this likelihood, maximizes the sum in the last line of this equation. Therefore, the maximum-likelihood estimator,  $\hat{p}$ , is the value of  $p$  for which the derivative of this sum with respect to  $p$  equals 0. This value is

$$\hat{p} = \frac{\sum_{k=0}^{N-1} [s(k\Delta) \cdot Du(k\Delta)]}{\sum_{k=0}^{N-1} s^2(k\Delta) \cdot \Delta}. \quad (16)$$

Substituting  $Du(k\Delta)$  from (14) into (16) shows that indeed  $\hat{p}$  converges to  $p$ , because  $s(k\Delta)$  and  $Dw(k\Delta)$  are mutually independent. In Sections IV and V,  $\hat{p}$  is expressed as a percentage, SW%.

Fig. 1 shows how to reconstruct  $Du(k\Delta)$  that is required for the computation of (16). Applying the inverse of  $L(s)$ , that is  $L^{-1}(s)$ , to the EEG and subsequent integration would give  $x \cdot u(t)$ . The discrete-time equivalent,  $x \cdot u(k\Delta)$ , is obtained by applying the bilinear transformation [19], [20, chapters 4.0 and 5.1.3] to  $L^{-1}(s)/s$ . Subtracting subsequent samples of  $x \cdot u(k\Delta)$  then results in the following algorithm for obtaining  $x \cdot Du(k\Delta)$  from the EEG samples,  $e(k\Delta)$ :

$$\begin{aligned} x \cdot Du(k\Delta) &= c_0 \cdot e(k\Delta + \Delta) + c_1 \cdot e(k\Delta) \quad \text{with} \\ c_0 &= \Delta/2 + 1/(2\pi\varphi_c) \quad \text{and} \\ c_1 &= \Delta/2 - 1/(2\pi\varphi_c) \end{aligned} \quad (17)$$

in which  $\varphi_c$  is the prewarped  $f_c$  [see (19)].

Fig. 1 also shows how to reconstruct  $s(k\Delta)$  that is also required for the computation of (16). Applying the inverse of  $L(s)$ , that is  $L^{-1}(s)$ , to the EEG and subsequent filtering by

$G(s)$  would give  $x \cdot s(t)$ . The discrete-time equivalent,  $x \cdot s(k\Delta)$ , is obtained by applying the bilinear transformation to  $L^{-1}(s) \cdot G(s)$ . The transformed filter for obtaining  $x \cdot s(k\Delta)$  from the EEG samples,  $e(k\Delta)$ , reads

$$x \cdot s(k\Delta) = a_1 \cdot x \cdot s(k\Delta - \Delta) + a_2 \cdot x \cdot s(k\Delta - 2\Delta) \\ + b_0 \cdot e(k\Delta) + b_1 \cdot e(k\Delta - \Delta) + b_2 \cdot e(k\Delta - 2\Delta)$$

with

$$a_1 = [8 - 2(2\pi\varphi_0\Delta)^2] \\ / [4 + (2\pi\varphi_0\Delta)^2 + 4\pi B\Delta] \\ a_2 = [-4 + 4\pi B\Delta - (2\pi\varphi_0\Delta)^2] \\ / [4 + (2\pi\varphi_0\Delta)^2 + 4\pi B\Delta] \\ b_0 = 4\pi B \left[ +\frac{1}{\pi\varphi_c} + \Delta \right] \\ / [4 + (2\pi\varphi_0\Delta)^2 + 4\pi B\Delta] \\ b_1 = 4\pi B \left[ -\frac{2}{\pi\varphi_c} \right] \\ / [4 + (2\pi\varphi_0\Delta)^2 + 4\pi B\Delta] \\ b_2 = 4\pi B \left[ +\frac{1}{\pi\varphi_c} - \Delta \right] \\ / [4 + (2\pi\varphi_0\Delta)^2 + 4\pi B\Delta] \quad (18)$$

in which  $\varphi_0$  and  $\varphi_c$  are the prewarped  $f_0$  and  $f_c$ , respectively. The prewarped frequencies,  $\varphi$ , in (17) and (18) are computed from the original frequencies,  $f$ , as follows [20, pages 208 and 217]

$$\varphi = [\tan(\pi f\Delta)]/\pi\Delta. \quad (19)$$

The reconstructed  $x \cdot Du(k\Delta)$  and  $x \cdot s(k\Delta)$ , and not  $Du(k\Delta)$  and  $s(k\Delta)$ , are used for the computation of (16). Since the unknown factor  $x$  occurs in both the numerator and the denominator of (16), this does not influence the estimate. For the same reason, scaling and calibration of the EEG signal is not required.

The estimator of (16) basically computes which fraction of the present  $s(k\Delta)$  is present in the future increment,  $Du(k\Delta) = u(k\Delta + \Delta) - u(k\Delta)$ . There is a time delay of  $\Delta/2$  between  $s(k\Delta)$  and  $Du(k\Delta)$ . This effect slightly biases the estimator because, in practice,  $s(k\Delta)$  is not completely constant during this interval. Extrapolating  $s(k\Delta)$  by  $\Delta/2$  into the future reduces this bias. This extrapolation must not involve  $e(k\Delta + \Delta)$  because that would cause dependency on the white noise component of  $Du(k\Delta)$ . As mentioned with (16), such dependency would bias the estimator. Therefore,  $x \cdot s(k\Delta + \Delta/2)$  was estimated as follows. First,  $x \cdot s(k\Delta)$  is computed by the filter of (18). Then, the same filter is extrapolated by  $\Delta$  and without input signal, in order to predict  $x \cdot s(k\Delta + \Delta)$  as follows:

$$x \cdot \overline{s(k\Delta + \Delta)} = a_1 \cdot x \cdot s(k\Delta) + a_2 \cdot x \cdot s(k\Delta - \Delta). \quad (20)$$

Finally,  $x \cdot s(k\Delta + \Delta/2)$  is estimated by linear interpolation as follows:

$$x \cdot \hat{s}(k\Delta + \Delta/2) = \frac{x \cdot s(k\Delta) + x \cdot \overline{s(k\Delta + \Delta)}}{2} \quad (21)$$

and replaces  $s(k\Delta)$  in the computation of equation (16).

Equation (21) predicts the slow-wave component produced by  $G(s)$  that might enter the next observation,  $Du(k\Delta)$ . The fraction of this component that will actually enter  $Du(k\Delta)$  depends on the feedback gain,  $p$ . Equation (16) estimates which fraction of the slow wave component continues (through the feedback loop) into the next observation. This is why we have named this fraction the slow-wave “microcontinuity.” (SW%) According to the model, this is an estimate of the neuronal *feedback gain*, which is related to sleep depth.

In some biomedical research environments, anti-aliasing measures are taken routinely and unconditionally in applications in which signals are sampled. We have purposely not done this, and we want to explicitly state our reasons in the following. Pre-sampling anti-aliasing filters would color the noise: they make the mutually independent increments  $dw(k\Delta)$  in  $du(k\Delta)$  depend on previous increments and, therefore, on  $s(k\Delta)$ . As mentioned earlier, this would bias the estimator. A similar effect occurs if the sampling frequency is too high: high-frequency low-pass filters that are present in any electronic and physiological system would also color the white noise. In practical applications, such bias by anti-aliasing filters can be substantial [10], [12, chapter 6.1]. Also, because any additional EEG rhythms are below 20 Hz, there is very little power above 25 Hz. The 90% spectral edge is even below 10 Hz [21]. Thus, we did not apply anti-aliasing filters.

This decision is supported by the fact that the formally derived optimal estimator does not include anti-aliasing filtering. In order to understand this better, we have verified how the analyzer processes frequencies exceeding the Nyquist frequency (in this application 25 Hz). These frequencies are much larger than  $f_0$  and  $f_c$  (1.0 Hz and 1.8 Hz, respectively). At these frequencies, the feedback through  $G(f)$  hardly contributes to the output signal and the low-pass filter,  $L(f)$ , acts as an integrator. Therefore, the remaining EEG model simply integrates white noise,  $\dot{w}(t)$ , in continuous time. Therefore, the resulting “EEG,”  $e(t)$  is a continuous-time Wiener process [18, chapter 4.4]. The microcontinuity analysis starts with sampling this process and filtering the samples by equations (17) and (18). Because  $\Delta \ll 1/\pi\varphi_c$ , the filter parameters  $c_0 = -c_1$  and  $b_0 = -2b_1 = b_2$ . This implies that both filters first compute the discrete-time increments,  $e(k\Delta) - e(k\Delta - \Delta)$ , and then process these increments further. These increments are the increments of the continuous-time Wiener process,  $e(t)$ , and therefore, by definition, discrete-time white noise [18, chapters 4.3 and 4.4], which is exactly limited to the Nyquist frequency. The gain of filter (17),  $1/2\pi f_c$ , exactly compensates the gain of the continuous time integrator,  $2\pi f_c$ . Therefore, the standard white noise,  $\dot{w}(t)$ , in the model is replaced by standard discrete-time white noise,  $Du(k\Delta)/\Delta$  in the analyzer. Both have a power spectral density of 1. This shows that the first-order roll-off of the continuous-time low-pass filter  $L(s)$ , followed by the sampling and

discrete-time filtering, acts as a perfect anti-aliasing filter on the white noise component.

#### IV. SMOOTHING, ARTIFACT REJECTION, AND (RELATIVE) POWER

Equation (16) shows that smoothing must be applied separately to numerator and denominator of the estimator. Such smoothing is not essential to the theory: the basic time resolution of the analysis equals the sampling interval (for an application, see [10]). In particular, the time resolution of the estimator is not limited by the low-frequency content of the slow waves. However, in the present application, some smoothing can be applied in order to reduce the noise which is introduced by  $dw(t)$ , while still preserving the dynamics of  $p(t)$ . We have tried several smoothing principles and obtained the best results [6] with the following recursive smoothers. Theoretically [22], such smoothers are optimal if  $p(t)$  represents the state of a Markov chain. The recursive smoothing procedure is as follows.

Using the reconstructed model signals of (17) and (21), the summations in (16) were computed over each 1s interval (with interval counter,  $n$ ), i.e.,

$$\begin{aligned} SU(n) &= \sum [x \cdot \hat{s}(k\Delta + \Delta/2) \cdot x \cdot Du(k\Delta)] \\ SS(n) &= \sum [x \cdot \hat{s}(k\Delta + \Delta/2)]^2 \cdot \Delta. \end{aligned} \quad (22)$$

These sums were recursively smoothed forward in time, starting at the beginning of the EEG recording

$$\begin{aligned} SU^+(n) &= (1-r) \cdot SU^+(n-1) + r \cdot SU(n) \\ SS^+(n) &= (1-r) \cdot SS^+(n-1) + r \cdot SS(n) \end{aligned} \quad (23)$$

and also backward in time, starting at the end of the EEG recording

$$\begin{aligned} SU^-(n) &= (1-r) \cdot SU^-(n+1) + r \cdot SU(n) \\ SS^-(n) &= (1-r) \cdot SS^-(n+1) + r \cdot SS(n). \end{aligned} \quad (24)$$

Initial values were set to 0. The contribution of each second of data,  $SU(k)$  and  $SS(k)$ , to the smoothed results decays by a factor of  $(1-r)$  at each recursion. Summing the forwardly and backwardly smoothed parameters,  $SU^+(n-1) + SU^-(n)$  and  $SS^+(n-1) + SS^-(n)$ , results in a time-symmetric weighted average at time  $n$  over all recorded data. The weight decays exponentially with increasing distance from  $n$ . The smoothing effect becomes weaker with increasing rate  $r$ . The data in this article were computed using the rate  $r = 0.01666$ . For this value of  $r$ , both (forward and backward) smoothers have a window size of  $\ln(0.5)/\ln(1-r) = 41$  s. That is, data farther than 41 s away from  $n$  weigh less than 50% of the data at  $n$ . For severe sleep apnea patients, who may enter deep sleep in a few seconds, a higher rate is probably more appropriate. We have replaced the summations of equation (16) by these time-symmetric recursive smoothed parameters. This results in better noise reduction and preservation of the dynamics of the feedback gain. We have also

multiplied the result by 100 in order to express the estimated microcontinuity as a percentage

$$SW\%(n) = 100 \cdot \frac{SU^+(n-1) + SU^-(n)}{SS^+(n-1) + SS^-(n)}. \quad (25)$$

The smoothed estimate of the power of the rhythmic component as applied in this article is computed in a similar way as follows:

$$SWP(n) = [SS^+(n-1) + SS^-(n)]/2. \quad (26)$$

This computation of power is rather traditional: the bandpass filtering of (18) from 0.5–2 Hz is followed by the squaring of (22) and smoothing [Eqs. (23), (24), (26)]. It is influenced [see (22)] by the amplification factor,  $x$ , which can introduce individual nonsleep-related effects in the EEG (Fig. 1). For well-smoothed estimates this influence can be derived from (12). It reads

$$SWP(n) = \frac{\pi B \cdot x^2}{1-p(n)} = \frac{\pi B \cdot x^2 \cdot 100\%}{100\% - SW\%(n)}. \quad (27)$$

This equation shows that the power, SWP, is composed of a nonsleep-dependent factor,  $SW0 = \pi B \cdot x^2$ , multiplied by a sleep-dependent factor,  $100\%/(100\% - SW\%)$ . According to (27), the nonsleep-dependent factor can be estimated at each second,  $n$ , from SW% and SWP as follows:

$$SW0(n) = SWP(n) \cdot \frac{100\% - SW\%(n)}{100\%}. \quad (28)$$

The automatic artifact rejection algorithm assumes that EEG activity behaves according to the model and artifacts do not. In particular, EEG activity should obey model equations (8) and (12), which implies that (with integrations over 1 s intervals and  $E$  being the expectation operator)

$$\begin{aligned} & \left[ \int s^2(t) dt - \int s(t) du(t) \right] \\ &= E \left[ \int s^2(t) dt - p \cdot \int s^2(t) dt - \int s(t) dw(t) \right] \\ &= (1-p) \cdot E \left[ \int s^2(t) dt \right] \\ &= \pi B \end{aligned} \quad (29)$$

which is independent of the value of  $p(t)$ . The discrete time equivalent includes the unknown amplification factor,  $x$ , and reads

$$E[SS(n) - SU(n)] = \pi B \cdot x^2. \quad (30)$$

Most artifacts do not behave according to the model and have been found to make  $[SS(n) - SU(n)]$  differ strongly from  $\pi B \cdot x^2$ . Therefore, we designed the automatic artifact rejection procedure as follows. The expression  $[SS(n) - SU(n)]$  is computed at each second,  $n$ . A whole-night histogram of the obtained values always shows a clear peak, which we interpret as the expected value of the expression and, therefore, equate with  $\pi B \cdot x^2$ . During high-frequency artifacts such as EMG the values obtained are positive and usually exceed  $\pi B \cdot x^2$  by at

least  $9\pi B \cdot x^2$  (they are at least  $10\pi B \cdot x^2$ ). During low-frequency artifacts such as moving electrodes the values obtained are negative and usually exceed  $\pi B \cdot x^2$  by at least  $-9\pi B \cdot x^2$  (they are more negative than  $-8\pi B \cdot x^2$ ). These thresholds at  $\pi B \cdot x^2 \pm 9\pi B \cdot x^2$  were determined experimentally in a previous unpublished study using other recordings. Artifacts are automatically detected when a threshold is crossed. When an artifact is detected, the inputs,  $SU(n)$  and  $SS(n)$ , to the smoothers of (23) and (24) are set to zero. This makes these smoothers interpolate between the adjacent artifact-free periods.

In order to compare our results to those that can be obtained by relative-power analysis, we computed power spectral density at a 1-minute time resolution as follows (frequency,  $f$ , and minute counter,  $M$ ). FFT-based power spectral density,  $PSD(M, f)$ , was computed by 10.24 s intervals and averaged over six intervals (the last one truncated in order to arrive at exactly 60 s). Relative SWP plots, RSWPs and RSWPw, based on a small and a wide slow-wave frequency band respectively, were computed as follows.

$$RSWP_s(M) = \frac{\sum_{f=0.5}^{2.0 \text{ Hz}} PSD(M, f)}{\sum_{f=0.5}^{20 \text{ Hz}} PSD(M, f)}$$

and

$$RSWP_w(M) = \frac{\sum_{f=0.25}^{4.0 \text{ Hz}} PSD(M, f)}{\sum_{f=0.25}^{20 \text{ Hz}} PSD(M, f)}. \quad (31)$$

#### V. SLOW-WAVE MICROCONTINUITY COMPARED TO SLOW-WAVE POWER: EFFECTS OF TIME OF NIGHT, AGE, GENDER, AND TEMAZEPAM

In a study [23] of the pharmacodynamics of temazepam (a benzodiazepine which promotes NREM-sleep duration), EEG (PzOz derivation) was recorded throughout two nights in 22 subjects. The recorder was a digital telemetric system [24], [25] with frequency response range (3-dB points) 0.03–1000 Hz, 14-bit sampling at 100 Hz per signal, and a total noise level of  $2\text{-}\mu\text{V}$  p-p. The subjects were grouped by age and gender (F: females, M: males) as follows: 18–34 years (6F, 4M), and 35–78 years (9F, 3M). Each subject took 20 mg of temazepam on one of the two nights (randomized, double blind, cross-over). Sleep stages were scored manually, using additionally recorded signals, and according to the standard scoring rules of Rechtschaffen and Kales [17].

The slow-wave analyzer automatically monitored at a 1 s time resolution the SWP (26) and its two components; the sleep-dependent SW% (25) and the nonsleep-dependent factor (28), SW0. The result was a SWP, SW%, and SW0 plot for each recorded night (Fig. 2).

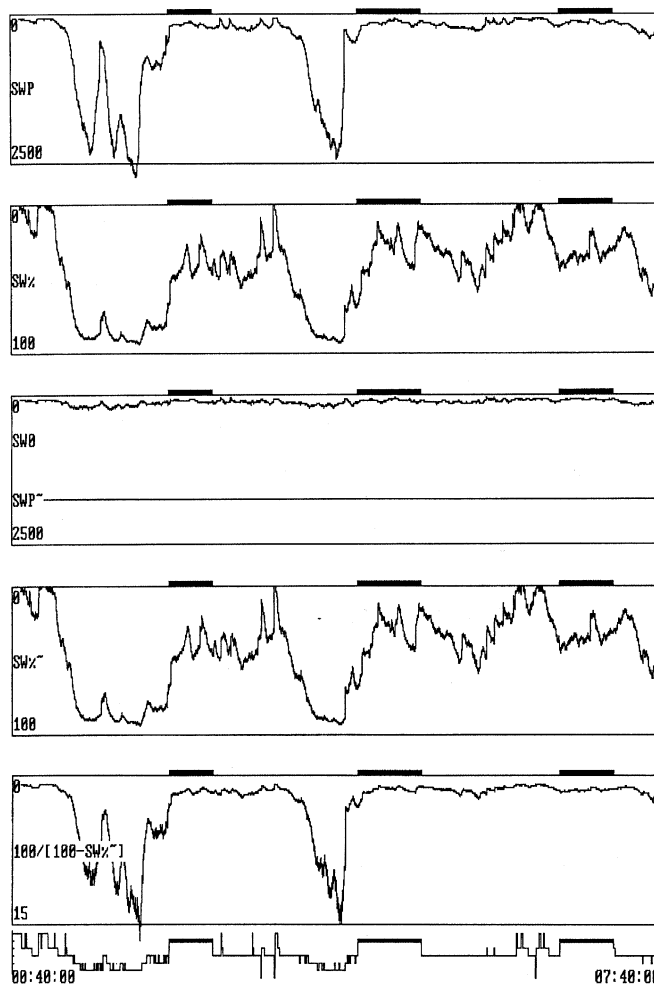


Fig. 2. The seven-hour sleep period of a male, aged 20, under placebo condition (sleep-wake recording 7141/94). From top to bottom six charts, each one with solid bars indicating the REM sleep periods. Chart 1: EEG (PzOz), SWP, in  $(\mu\text{V})^2$ . Chart 2: EEG slow-wave feedback gain, i.e., SW%, which is the fraction of the present slow wave that is transferred to the near-future EEG. Chart 3 (top trace): SW0 in  $(\mu\text{V})^2$ , the part of the SWP variations in chart 1 that the model could not predict from SW%. Chart 3 (bottom trace) illustrates that dynamic attenuation of the EEG amplitude by the square root of SWP (chart 1) removed all variations from the resulting SWP, SWP. Chart 4: EEG slow-wave feedback, SW%, computed from the thus dynamically attenuated EEG. Note that despite this attenuation, charts 2 and 4 are identical, which implies that SW% only depends on EEG shape, not amplitude. Chart 5: neuronal power variations as reconstructed by model equation (27) from SW% in chart 4. Note that charts 1 and 5 are almost identical, which implies that the original neuronal power variations are almost fully coded in the shape of the EEG. Note also from the scales of charts 1 and 5 that the *absolute* values of neuronal power could not be reconstructed because of the unknown factor  $x$  (we assumed  $SW0(n) = 1$  in the reconstruction). Chart 6: traditional manual classification (R&K) into (from top to bottom) the six sleep stages: Wakefulness, REM sleep (bold), drowsiness, and the increasingly deep NREM sleep stages 2, 3, and 4. Note that removing all power variations from the EEG (chart 3) did not affect the dynamics of microcontinuity (chart 4). Note also that the model can even reconstruct the original power variations (chart 5).

Fig. 2 illustrates that the well-known night-time dynamics in SWP are fully coded in SW%. Charts 2 and 4 illustrate that SW% depends only on the shape of the EEG, not on amplitude: chart 2 shows the microcontinuity as computed directly from the EEG while chart 4 is computed in the same way but after attenuation of the EEG by the dynamic SWP plot. This attenuation completely removed the power fluctuations from the EEG

(see chart 3). Still, charts 2 and 4 are identical. This implies that SW% analysis is indeed independent of the EEG amplitude and that the night-time dynamics in SWP are fully coded in the microcontinuity (shape) of the EEG. The latter is also demonstrated by chart 5. This chart shows that the model can reconstruct the original neuronal-power fluctuations even after removal of all EEG-power variations!

These illustrations are consistent with the model, which predicts that sleep-related variations in SWP are caused by variations in slow-wave feedback, SW%. Objective validation of this prediction was based on computation of the whole-night correlation between the SW% and SWP plots in each subject. The relationship (28) between SW% and SWP is nonlinear, which would bias the correlation analysis (and also ANOVA [6]). Therefore, the relationship was first linearized by logarithmic transformation as follows:

$$\ln[\text{SWP}(n)] = \ln[\text{SW0}(n)] - \ln \left[ \frac{100\% - \text{SW}\%_0(n)}{100\%} \right]. \quad (32)$$

According to the model, the variations in  $\ln[\text{SWP}(n)]$  and  $\ln[(100\% - \text{SW}\%_0(n))/100\%]$  should be highly correlated. In order to test this, the whole-night correlation coefficient between these logarithmically transformed plots was computed for each of the 44 recorded nights. The mean, the 95%-confidence interval of the mean (both obtained using the Fisher  $Z$ -transform) and the range of this correlation coefficient were found to be 0.961, (0.954 to 0.967), and (0.89 to 0.99), respectively.

The effects of age and temazepam on SWP are at least partly due to a real effect on sleep depth [6], [23]. Gender also affects SWP, but probably not sleep depth [5], [6]. In that case, SW% should only show the effects of age and temazepam. In order to test this, we analyzed the effects of age, temazepam, and gender on maximum sleep depth. The moment of maximum sleep depth was detected from the SWP-plot: it is the moment where the SWP-plot (for an example, see chart 1 in Fig. 2) reaches its largest value. Maximum sleep depth is characterized by the linearized (see above) values  $\ln[\text{SWP}]$ ,  $\ln[\text{SW0}]$  and  $\ln[(100\% - \text{SW}\%)/100\%]$  at that moment. For comparison, maximum sleep depth was also obtained by taking the whole-night maximum from each one of the relative-power plots, RSWPs and RSWPw. Age and gender effects on all these values were analyzed by ANOVA. Temazepam effects were analyzed using the  $t$ -test. The results are summarized in Table I.

Temazepam was found to reduce maximum sleep depth as characterized by both SWP and SW% (both  $p$  values  $<0.005$ ), but not by SW0, RSWPs, or RSWPw (the three  $p$  values  $>0.5$ ). In both the placebo and the temazepam nights, increased age reduced maximum sleep depth as characterized by SWP (both  $p$  values  $<0.001$ ), SW% (both  $p$  values  $<0.01$ ) and SW0 (both  $p$  values  $<0.04$ ), but not by RSWPs and RSWPw (the four  $p$  values  $>0.15$ ). In both the placebo and the temazepam night, females had significantly larger maxima of SWP and SW0 (the four  $p$  values  $<0.01$ ) but not of SW%, RSWPs, and RSWPw (the six  $p$  values  $>0.2$ ).

Temazepam affects the total duration of NREM sleep as traditionally defined [17] and also improves a subject's

TABLE I  
SIGNIFICANCE LEVELS OF THE EFFECTS OF AGE, GENDER AND TEMAZEPAM ON WHOLE-NIGHT MAXIMA OF BOTH RSWPs AND RSWPw, SWP AND ITS TWO COMPONENTS, SLOW WAVE FEEDBACK (SW%) AND NONSLEEP-RELATED ATTENUATION (SW0). NOTE THAT TEMAZEPAM AND GENDER AFFECT SWP EXCLUSIVELY THROUGH SW% AND SW0, RESPECTIVELY. AGE SEEMS TO AFFECT SWP THROUGH BOTH SW% AND SW0

	RSWPs	RSWPw	SWP	SW%	SW0
Age	.26	.15	.001	.01	.04
Gender	.22	.77	.01	.5	.01
Temazepam	.59	.51	.005	.005	.71

TABLE II  
QUESTIONS FOR ASSESSING SSQ. THE ORIGINAL QUESTIONNAIRE WAS IN DUTCH. AFTER EACH POLYGRAPHIC SLEEP/WAKE RECORDING, THE SUBJECT ANSWERED EACH QUESTION BY MARKING THE "YES" OR THE "NO" BOX. IN THE EXAMPLE BELOW, THE MARKINGS WERE MADE BY A "PERFECT" SLEEPER, RESULTING IN THE MAXIMUM SSQ OF 16

	yes	no
1 I slept deeply last night	x	
2 I feel I slept very badly last night		x
3 I was awake more than half an hour before falling asleep last night		x
4 I woke up several times last night		x
5 After waking up this morning, I felt tired		x
6 I did not have enough sleep last night		x
7 I got out of bed last night		x
8 After waking up this morning, I felt well-rested	x	
9 I feel I slept only a few hours last night		x
10 I feel I slept well last night	x	
11 I did not sleep a wink last night		x
12 I fell asleep easily last night	x	
13 I woke up last night and could hardly get back to sleep (If you did not wake up at all last night, answer "no")		x
14 I was restless last night		x
15 I had less than five hours sleep last night		x
16 My sleep was affected by the recording		x

personal assessment of sleep quality [26], [27]. However, an intra-subject correlation between the effect on the subjective sleep quality and the effect on the total duration of NREM-sleep has never been reported. This may be due to the fact that these durations were commonly computed through thresholding overnight SWP plots or manually scored sleep stage plots [17]. Both plots depend on SWP which is also influenced by nonsleep dependent factors as mentioned in Sections I, II and IV. Fixed power or sleep stage thresholds then correspond to different sleep depths in different subjects. We investigated whether thresholding SW% plots is a better way to detect such correlations. For comparison, we have computed durations based on thresholding SWP plots, relative-power (RSWPs and RSWPw) plots, and manually scored stage (R&K) plots. SW%-duration, SWP-duration, RSWPs-duration, RSWPw-duration and R&K-duration were defined as the number of minutes with SW% exceeding 7%, SWP exceeding  $60 (\mu V)^2$ , RSWPs exceeding 0.49, RSWPw exceeding 0.76, and R&K exceeding stage 1, respectively. These thresholds were automatically selected in such a way that the summed (over all subjects and nights) durations were each equal to the summed NREM-sleep durations as defined by the R&K plots (i.e., the total time spent in sleep stages 2, 3 and 4). Subjective sleep quality, (SSQ), was defined as the number of questions of a 16-item questionnaire (Table II) answered in favor of "good sleep." Correlations between temazepam effects (i.e., temazepam-placebo difference) were evaluated using the bivariate Pearson correlation coefficient,  $\rho$ . The temazepam

effect on sleep quality was found to be significantly correlated ( $\rho = 0.42$ ,  $p < 0.05$ ) with the effect on SW%-duration, not with the effects on SWP, RSWPs-, RSWPw-, or R&K-duration (the four  $\rho$  values were 0.22, 0.36, 0.21, and 0.32 respectively. The four  $\rho$  values  $> 0.1$ ).

## VI. CONCLUSION

SW% is, by definition (16), the fraction of the currently present slow wave that is continued in the near-future EEG. Continuation of current activity into the future essentially implies a temporal feedback mechanism. The fact that we found clear time-of-night variations in SW%, therefore, inevitably implies the existence of a slow-wave generating closed loop in which the feedback gain varies in the course of the night. Reasoning based on physiology, neuronal feedback gain was also found [7]–[9] to be the dynamic physiological state representing NREM-sleep depth. These two independent lines of evidence strongly suggest that NREM-sleep depth corresponds to the feedback gain of neuronal slow-wave oscillating loops.

A simple model of this principle suggests that variations in SWP are due to variations of sleep-related microcontinuity, according to the multiplicative relationship given in (28). Our data support the model because we indeed found strong correlations (0.89 to 0.99) between logarithmically transformed whole-night power and microcontinuity plots (see also Fig. 2).

Our data confirm previously reported effects of age, temazepam and gender on SWP. But only age and temazepam, not gender, affected SW%. This suggests that age and temazepam affect real sleep depth but gender affects SWP through a nonsleep-related (possibly anatomical) process. These results support an independent study [5] suggesting that the gender effect on SWP is not due to a gender effect on physiological sleep depth.

These results also suggest that the microcontinuity analysis can distinguish sleep-related from nonsleep-related effects on SWP. In that case, SW% is a more accurate estimator of sleep depth than SWP is. This suggestion was confirmed by the fact that the effects of temazepam on SSQ correlated to SW%-duration, not to SWP-duration.

Similar to SW%, both RSWP plots should not be affected by anatomical parameters that do affect SWP. Indeed, gender had no effect on RSWP-maximum. Also, SSQ was more strongly correlated to RSWPw-duration than to SWP-duration. However, the correlation between SSQ and SW%-duration was still higher. Also, RSWP-maximum failed to detect the age and temazepam effects that were detected by SW%-maximum. Inspection of the plots showed that the superiority of the SW% measure is partly due to the relatively high sensitivity of RSWP to low-frequency electrode artifacts that are caused by movements of the subject. In contrast, the denominator,  $s(k\Delta) \cdot Du(k\Delta)$ , of the SW% estimator uses the phase information in the EEG. This makes the analyzer respond differently to slow waves than to low-frequency artifacts, even when the two have indistinguishable power spectral densities. Additionally, the model-based artifact detector discussed with (30) was found to reject such low-frequency and other artifacts very well, as was already discovered in earlier studies: see for instance Fig. 3 in [13] and “the synchronization model” in Fig. 3 in [28]. RSWP measures may also improve by some

method of rejecting these artifacts from the analysis. However, a considerable advantage of SW% in detecting effects on sleep will remain that SW% is computed in the time domain and, therefore, offers a much better time resolution. This is important when neuronal feedback gain can change rapidly, such as in sleep apnea patients or in other applications such as alpha-blocking [10], the detection of K-complexes [29] and the cycling alternating pattern (CAP) in sleep [30].

The formal derivation of the analyzer precludes the use of anti-aliasing filters. Therefore, not-modeled high-frequency signal generators such as muscle artifacts may bias the results. Although the model-based artifact rejection of paragraph IV handles these artifacts very well, not all artifacts will be rejected. Therefore, more practical experience must assert whether or when this is a serious problem. The results discussed above indicate that this was not the case in the present study.

Recent physiological evidence [31] shows that different frequencies within the slow-wave range may point to different mechanisms of sleep. Components, the slow component ( $< 1$  Hz) and the delta component (1–4 Hz), are the result of different feedback mechanisms. But both mechanisms have a feedback gain that increases with increasing sleep depth. This may partly explain the success of methods, including the microcontinuity estimator, that roughly cover both frequency bands. Still, because physiological research suggests the existence of functionally different frequency bands in the slow-wave range, a next step should be to apply the microcontinuity analysis separately to the two EEG components.

In the same reference [31], it was argued that EEG analysis “should take into consideration the actual aspect of waves and, if possible, their relationship with the state of the cellular aggregates of the corticothalamic network” underlying slow waves. The microcontinuity estimator is the first method that does both. As a consequence, microcontinuity allows a physiological interpretation: it reflects the degree of activation of the low-frequency neuronal feedback loops that generate the slow waves in the EEG.

## ACKNOWLEDGMENT

The authors would like to thank A. Janssen and M. Roessen who made the recording hardware and software and R. Biemond and E. Kemp who made most of the recordings.

## REFERENCES

- [1] A. A. Borbély and P. Achermann, “Ultradian dynamics of sleep after a single dose of benzodiazepine hypnotics,” *Eur. J. Pharmacol.*, vol. 195, pp. 11–18, 1991.
- [2] I. Feinberg, “Changes in sleep cycle patterns with age,” *J. Psychiatr. Res.*, vol. 10, pp. 283–306, 1974.
- [3] I. Feinberg, J. D. March, G. Fein, T. C. Floyd, J. M. Walker, and L. Price, “Period and amplitude analysis of 0.5–3 c/sec activity in NREM sleep of young adults,” *Electroenceph. Clin. Neurophysiol.*, vol. 44, pp. 202–213, 1978.
- [4] D. J. Dijk, B. Hayes, and C. Czeisler, “Dynamics of electroencephalographic sleep spindles and slow wave activity in men: Effect of sleep deprivation,” *Brain Res.*, vol. 626, pp. 190–199, 1993.
- [5] D. J. Dijk, D. G. M. Beersma, and G. M. Bloem, “Sex differences in the sleep EEG of young adults: Visual scoring and spectral analysis,” *Sleep*, vol. 12, pp. 500–507, 1989.
- [6] M. S. Mourtazav, B. Kemp, A. H. Zwinderman, and H. A. C. Kamphuisen, “Age and gender affect different characteristics of slow waves in the sleep EEG,” *Sleep*, vol. 18, pp. 557–564, 1995.

- [7] M. Steriade, P. Gloor, R. R. Llinás, F. H. Lopes da Silva, and M.-M. Mesulam, "Basic mechanisms of cerebral rhythmic activities," *Electroenceph. Clin. Neurophysiol.*, vol. 76, pp. 481–508, 1990.
- [8] M. Steriade, "Basic mechanisms of sleep generation," *Neurology*, vol. 42(Suppl.6), pp. 9–17, 1992.
- [9] M. Steriade, D. A. McCormick, and T. J. Sejnowski, "Thalamocortical oscillations in the sleeping and aroused brain," *Science*, vol. 262, pp. 679–685, 1993.
- [10] B. Kemp, "Accurate measurement of flash-evoked alpha attenuation," *Electroenceph. Clin. Neurophysiol.*, vol. 56, pp. 248–253, 1983.
- [11] B. Kemp, P. Jaspers, J. M. Franzen, and A. J. M. W. Janssen, "An optimal monitor of the electroencephalographic sigma sleep state," *Biological Cybern.*, vol. 51, pp. 263–270, 1985.
- [12] B. Kemp, "Model-based monitoring of human sleep stages," Ph.D. dissertation, Dept. Electrical Engineering, Twente Univ. Technol., Enschede, The Netherlands, 1987.
- [13] B. Kemp, A. Värrí, A. da Rosa, K. D. Nielsen, J. Gade, and T. Penzel, "Analysis of brain synchronization, based on noise-driven feedback models," in *Proc. Annu. Int. Conf. IEEE Engineering in Medicine and Biology Society (IEEE-EMBS)*, vol. 13, 1991, pp. 2305–2306.
- [14] J. F. V. Caekebeke, J. G. Van Dijk, A. C. Rosa, and B. Kemp, "A model relating K-complexes to spontaneous slow-wave activity during sleep," in *Phasic Events and Dynamic Organization of Sleep*, M. G. Terzano, P. L. Halasz, and A. C. Declerck, Eds. New York: Raven, 1991, pp. 41–51.
- [15] B. Kemp, "Cerebral information processing estimated by unpredictability of the EEG," *Clin. Neurol. Neurosurg.*, vol. 94(Suppl.), pp. S103–S105, 1992.
- [16] B. Kemp and H. A. P. Blom, "Optimal detection of the alpha state in a model of the human electroencephalogram," *Electroenceph. Clin. Neurophysiol.*, vol. 52, pp. 222–225, 1981.
- [17] A. A. Rechtschaffen and A. Kales, "A manual of standardized terminology, techniques and scoring system for sleep stages of human subjects," Public Health Service, U.S. Government Printing Office, Washington, D.C., 1968.
- [18] H. J. Larson and B. O. Shubert, *Probabilistic Models in Engineering Sciences: Random Noise, Signals, and Dynamic Systems*. New York: Wiley, 1979, vol. 2.
- [19] B. Kemp and F. H. Lopes da Silva, "Model-based analysis of neurophysiological signals," in *Digital Biosignal Processing*, R. Weitkunat, Ed. Amsterdam, The Netherlands: Elsevier Science, 1991, pp. 129–155.
- [20] A. V. Oppenheim and R. W. Schaffer, *Digital Signal Processing*. Englewood Cliffs, NJ: Prentice-Hall, 1975.
- [21] J. Fell, J. Röschke, K. Mann, and C. Schäffner, "Discrimination of sleep stages: A comparison between spectral and nonlinear EEG measures," *Electroenceph. Clin. Neurophysiol.*, vol. 98, pp. 401–410, 1996.
- [22] B. Kemp, E. W. Gröneveld, A. J. M. W. Janssen, and J. M. Franzen, "A model-based monitor of human sleep stages," *Biological Cybern.*, vol. 57, pp. 365–378, 1987.
- [23] B. Tuk, J. J. L. Oberyé, M. S. M. Pieters, H. C. Schoemaker, B. Kemp, J. van Gerven, M. Danhof, H. A. C. Kamphuisen, A. F. Cohen, D. D. Breimer, and C. C. Peck, "Pharmacodynamics of temazepam in primary insomnia: assessment of the value of quantitative EEG and saccadic eye movements in predicting improvement of sleep," *Clin. Pharmacol. Ther.*, vol. 62, no. 4, pp. 444–452, 1997.
- [24] B. Kemp, A. J. M. W. Janssen, and M. J. Roessen, "A digital telemetry system for ambulatory sleep recording," in *Sleep-Wake Research in The Netherlands*, A. M. L. Coenen and J. Arends, Eds. Utrecht, The Netherlands: Drukkerij Elinkwijk, 1993, vol. 4, pp. 129–132.
- [25] B. Kemp, A. J. M. W. Janssen, M. J. Roessen, and H. A. C. Kamphuisen, "A digital telemetric system for sleep polygraphy," *J. Sleep Res.*, vol. 3(Suppl.1), p. 126, 1994.
- [26] F. Fraschini and B. Stankov, "Temazepam: Pharmacological profile of a benzodiazepine and new trends in its clinical application," *Pharmacol. Res.*, vol. 27, pp. 97–113, 1993.
- [27] R. C. Heel, R. N. Brogden, T. M. Speight, and G. S. Avery, "Temazepam: A review of its pharmacological properties and therapeutic efficacy as an hypnotic," *Drugs*, vol. 21, pp. 321–340, 1981.
- [28] B. Kemp, A. Värrí, A. C. Rosa, K. D. Nielsen, and J. Gade, "A simple format for exchange of digitized polygraphic recordings," *Electroenceph. Clin. Neurophysiol.*, vol. 82, pp. 391–393, 1992.
- [29] A. C. Rosa, B. Kemp, T. Paiva, F. H. Lopes da Silva, and H. A. C. Kamphuisen, "A model-based detector of vertex waves and K complexes in sleep electroencephalogram," *Electroenceph. Clin. Neurophysiol.*, vol. 78, pp. 71–79, 1991.
- [30] A. C. Rosa, L. Parrino, and M. G. Terzano, "Automatic detection of cyclic alternating pattern (CAP) sequences in sleep: Preliminary results," *Clin. Neurophysiol.*, vol. 110, pp. 585–592, 1999.

- [31] F. Amzica and M. Steriade, "Electrophysiological correlates of sleep delta waves," *Electroenceph. Clin. Neurophysiol.*, vol. 107, pp. 69–83, 1998.



**Bastiaan (Bob) Kemp** (A'95–M'95) was born in 1951 in The Netherlands. He received the M.Sc. degree in electrical engineering and the Ph.D. degree in model-based monitoring of sleep stages from Twente University of Technology, Enschede, The Netherlands, in 1977 and 1987, respectively.

He is a Medical Physicist in the Department of Neurology at Leiden University Medical Centre, Leiden, The Netherlands. He is also a Clinical Physicist and director of the Center for Sleep and Wake Disorders in MCH - Westeinde Hospital, Den Haag, The Netherlands. His interests are in sensors, models, and algorithms for the study of sleep and movement disorders.



**Aeilko (Koo) H. Zwiderman** was born in 1960 in The Netherlands. He received the M.Sc. degrees in both statistics and psychometry in 1985 from the University of Groningen, Groningen, The Netherlands, and the Ph.D. degree in estimation and testing problems with the Rasch model from the University of Nijmegen, Nijmegen, The Netherlands, in 1991.

He is currently an Associate Professor in the Department of Medical Statistics at Leiden University, Leiden, The Netherlands. His research interests include statistical models for correlated discrete and censored data, and statistical models for smoothing.



**Bert Tuk** was born in 1967 in The Netherlands. He received the M.Sc. degree in biopharmaceutical sciences in 1992 from the University of Leiden, Leiden, The Netherlands, and the Ph.D. degree in clinical pharmacology on the modeling of receptor mediated pharmacological responses at the University of Leiden and Stanford University, Stanford, CA, in 1998.

His research interests include the pharmacokinetic and pharmacodynamic modeling of drug effects and the simulation of clinical trials.



**Hilbert A. C. Kamphuisen** was born in 1931 in The Netherlands. He received the M.D. and Ph.D. degrees from the Medical Faculty of the University of Utrecht, Utrecht, The Netherlands, in 1955 and 1969, respectively.

He was a Full Professor in clinical neurophysiology at Leiden University, Leiden, The Netherlands, from 1972–1994 when he retired. He has published many articles and books about sleep and clinical neurophysiology, and some cultural subjects. He is one of the founders of the Centre for Sleep and Wake Disorders at MCH - Westeinde Hospital, Den Haag, The Netherlands.



**Josefien J. L. (Janine) Oberyé** was born in 1972 in The Netherlands. She received the M.Sc. in biopharmaceutical sciences at Leiden University, Leiden, The Netherlands, in 1996.

She is currently a Clinical Research Scientist at the Clinical Development Department of NV Organon, Oss, The Netherlands where she prepares a clinical development plan for infertility-related compounds including phase 2 and phase 3 studies. She prepares, initiates, manages and reports these studies. Her interests include infertility research (in general) and GnRH antagonists.